Journal of Power Sources 247 (2014) 1026–1032

Contents lists available at SciVerse ScienceDirect

Journal of Power Sources

journal homepage: www.elsevier.com/locate/jpowsour

Proposal of simple and novel method of capacity fading analysis using pseudo-reference electrode in lithium ion cells: Application to solvent-free lithium ion polymer batteries

Kumi Shono [a], Takeshi Kobayashi [a], Masato Tabuchi [b], Yasutaka Ohno [c], Hajime Miyashiro [a], Yo Kobayashi [a,*]

[a] Central Research Institute of Electric Power Industry, Tokyo 201-8511, Japan
[b] Daiso Co., Ltd., Hyogo 660-0842, Japan
[c] Electric Power Engineering Systems, Tokyo 201-8511, Japan

HIGHLIGHTS

- Proposal of a simple pseudo-reference electrode for lithium ion battery.
- Separation of the cathode/anode potential and impedance using pseudo-reference.
- >1000 cycles operation using $LiNi_{1/3}Mn_{1/3}Co_{1/3}O_2$, solvent-free SPE, and graphite.
- Continuous lithium loss at the graphite is the main factor of the capacity fading.

GRAPHICAL ABSTRACT

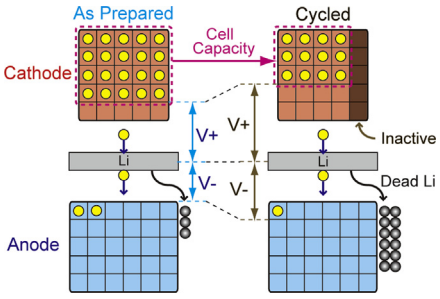

ARTICLE INFO

Article history:
Received 5 April 2013
Received in revised form
2 June 2013
Accepted 12 June 2013
Available online 22 June 2013

Keywords:
Lithium battery
Pseudo-reference electrode
Solid polymer electrolyte
Capacity fading

ABSTRACT

We propose a simple procedure for introducing a pseudo-reference electrode (PRE) to lithium ion batteries using isometric lithium metal placed between the cathode and anode, and we successfully obtained the cathode and anode voltage profiles, individual interfacial impedances, and the misalignment of the operation range between the cathode and anode after cycle operation. The proposed procedure is applicable to lithium ion battery systems using a solid electrolyte to prepare two cells with a lithium counter electrode. We determined the capacity decrease of a solvent-free lithium ion polymer battery consisting of a $LiNi_{1/3}Mn_{1/3}Co_{1/3}O_2$ (NMC), a polyether-based solid polymer electrolyte (SPE), and a graphite (Gr) with the proposed PRE over 1000 cycles. The capacity retention of the [Gr|SPE|NMC] cell reached 50% at the 1000th cycle upon the optimization of cell preparation, and we found that the main factor of the capacity decrease was the continuous irreversible loss of active lithium at the graphite anode, not the oxidation of the SPE. Our findings suggest that we should reconsider combining a polyether-based SPE with a conventionally used 4 V class cathode and a graphite anode to develop an innovative, safe, and low-cost battery for the expected large lithium ion battery systems for stationary use.

* Corresponding author. 2-11-1, Iwado-Kita, Komae, Tokyo 201-8511, Japan. Tel.: +81 3 3480 2111; fax: +81 3 3480 3401.
E-mail address: kobayo@criepi.denken.or.jp (Y. Kobayashi).

0378-7753/$ – see front matter © 2013 Elsevier B.V. All rights reserved.
http://dx.doi.org/10.1016/j.jpowsour.2013.06.071

1. Introduction

The application of lithium ion batteries has now begin to extend from mobile use to EV or stationary use. For such large systems, an operation life much longer than that of mobile systems is required. Thus, a complete understanding of the capacity fading mechanism of lithium ion batteries is important for the development of such long-life battery systems. Monitoring the voltage of the cell during charge and discharge is a basic approach to understanding electrode reactions inside the cell. However, as the anode materials in most lithium ion batteries have a potential slope, we cannot easily obtain the accurate potential of each electrode during operation.

The introduction of a reference electrode with a stable potential is a useful approach to monitoring the potential of each electrode in lithium ion cells [1–4]. However, the configuration of such cells designed to obtain a suitable reference electrode performance has not yet been optimized for the simple and long-term operation of the cells. One novel method of optimizing the configuration is to apply a lithium alloy material with a sufficiently fine (25 μm diameter) reference electrode [3]. Previous studies have successfully shown changes in the area specific impedance (ASI), the misalignment of electrode-capacity windows, and changes in the AC impedance during storage [5].

Our objective is to apply a solvent-free solid polymer electrolyte (SPE) in a lithium ion cell system [6,7]. The thickness of the SPE sheet used is 50 μm owing to its relatively low lithium ion conductivity. Therefore, we cannot use the so-called "beaker cell" because it requires a long electrolyte distance between electrodes. Furthermore, it is difficult to introduce the above-mentioned fine reference electrode into our system because of concerns regarding inhomogeneous current flow and the insufficient mechanical strength of the applied SPE. The distribution of current flow in the SPE requires stricter homogeneity than that in a liquid electrolyte because of the low lithium ion conductivity and immobility of the SPE.

With the above-mentioned restrictions, we propose a novel and simple lithium ion cell configuration, as shown in Fig. 1. Here, the anode is graphite (Gr) and the cathode is $LiNi_{1/3}Mn_{1/3}Co_{1/3}O_2$ (NMC). The anode and cathode are each encapsulated in a laminate pouch while facing isometric lithium metal, and each lithium electrode is externally connected outside the cells. This cell configuration can be described as [Gr|SPE|Li]–[Li|SPE|NMC], and an array of pair-type cells was named the "Nico-Ichi" -type cell. In the configuration, we can use not only laminate pouch-type cells but also coin-type cells. In the configuration, the lithium metal acts as a lithium ion deposition/dissolution bridge and also as a pseudo-reference electrode (PRE) during charge and discharge. The proposed procedure of introducing the reference electrode may be in contrast to the procedure of formally introducing such an electrode. In addition, we cannot recommend using the proposed procedure if the dendrite growth of the lithium metal and the increase in impedance due to the introduction of the additional lithium and electrolyte interface significantly affect the cell performance. However, the proposed system has many merits as follows: (i) the cathode and anode voltage profiles and their interfacial impedances can be obtained, (ii) a homogeneous current distribution is guaranteed inside the cell because the reference electrode faces isometric cathode and anode materials, (iii) the capacity of each electrode can be quantitatively determined during or after operation by measuring the capacity of each half cell, and (iv) the misalignment of the operated state of charge (SOC) can be monitored and the anode or cathode SOC can be adjusted by supplying or absorbing lithium ions from the facing lithium metal reference electrode. Furthermore, (v) we can also use different types of electrolyte in each half cell at different temperatures to determine the degradation factor fpr the combination of an electrode and electrolyte. We applied the proposed lithium ion cells with a lithium PRE in a 4 V class [Gr|SPE|NMC] system and determined the capacity fading mechanism of the cell by analyzing cell voltage profiles, impedance trends, and the remaining electrode capacities after cycle operations.

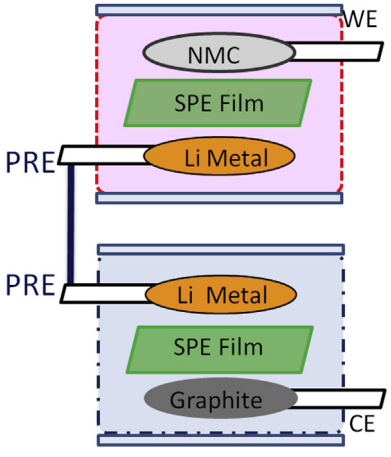

Fig. 1. Schematic of proposed array of pair-type lithium ion cells with pseudo-reference electrode (PRE): Nico-Ichi-type cell.

2. Experimental

2.1. Polymer structure

We used a conventional polyether-based material (Fig. 2) as the SPE sheet [P(EO/MEEGE/AGE) = 82/18/2 (Daiso) where EO is ethylene oxide, MEEGE is 2-(2-methoxyethoxy)ethyl glycidyl ether, and AGE is allyl glycidyl ether] [8]. Lithium bis(trifluoromethylsulfonyl)imide (LiTFSI, 3 M) was added to the SPE at a molar ratio of [O]/[Li] = 16/1. The thickness of the SPE sheet used was approximately 50 μm. In addition, another SPE without an AGE bridging group, [P(EO/MEEGE) = 88/12 (MW = 1.5 M)], was used at the SPE and electrode interface by overcoating the SPE dissolved in acetonitrile (AN) on the electrode. Details of the overcoating procedure were reported previously [9]. The lithium salts used were LiTFSI at the Gr|SPE interface and lithium tetrafluoroborate ($LiBF_4$) at the NMC|SPE interface to prevent the corrosion of the aluminum current collector induced by LiTFSI. The apparent ionic conductivity, which was obtained from R_S (ACσ), exhibited an order (10^{-4} S cm^{-1} at 333 K) similar to that in a previous report [10].

2.2. Electrode preparation

90.4 wt.% NMC was mixed with 6.4 wt.% conductive additives (3.2 wt.% carbon black and 3.2 wt.% VGCF®, Showa Denko) and a 3.1 wt.% water-based binder (2.1 wt.% carboxymethylcellulose; CMC and 1.0 wt.% styrene butadiene rubber; SBR). The choice of the

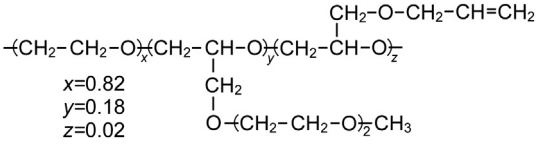

Fig. 2. Structure unit of SPE used.

CMC/SBR binder with a 4 V cathode may be unconventional. However, it improved the cycle performance in the SPE system. The obtained results are reported in detail elsewhere [11]. A similar improvement in cycle performance using a liquid electrolyte was reported by other groups [12]. A mixed slurry was pasted on aluminum foil. The slurry consisted of 95.1 wt.% graphite was mixed with 1.9 wt.% VGCF® and 2.9 wt.% water-based binder (1.9 wt.% CMC and 1.0 wt.% SBR). The mixed slurry was pasted on electrolytic copper foil. After sufficient drying for over 10 h at 373 K, followed by pressing and cutting (16 mm ϕ = 2 cm^2) of electrodes, the electrodes were introduced into a glove box (MIWA MFG Co., Ltd., H_2O < 0.1 ppm, O_2 < 0.4 ppm). Then, 10 wt.% SPE in AN was overcoated on the electrodes and dried at 353 K for over 10 h in vacuum.

2.3. Cell preparation and operation

SPE-overcoated NMC or graphite was placed facing the lithium metal (Honjo Metal, 0.3 mm t, 16 mm ϕ) through the 50 μm SPE sheet (20 × 20 mm^2). The cell was encapsulated in an Al laminate pouch (60 × 110 mm^2) at 373 K using a handy laminator in the glove box. The handy laminator used was modified from that used for stationery. In the case of the Nico-Ichi-type cell, each lithium electrode was connected through the current collector, as shown in Fig. 1, and used as a pseudo-reference electrode.

The Nico-Ichi-type cell consisting of [Gr|SPE|Li]–[Li|SPE|NMC] was operated between 2.5 and 4.2 V. A normal lithium ion cell consisting of [Gr|SPE|NMC] was also prepared for reference. The prepared cells were initially operated at a rate of C/24 for two cycles as formation cycles. Then, they were cycled in a protocol of (C/8 for two cycles and C/2 for 48 cycles) × n loops. The operation temperature was 333 K. The voltage profiles of graphite and NMC were monitored using a lithium PRE during charge and discharge. The active material weight ratio of graphite to NMC was approximately 1:2. The reversible capacities of graphite and NMC using a lithium counter electrode were 340 mAh g^{-1} (between 0 and 2.5 V) and 150 mAh g^{-1} (between 2.7 and 4.2 V), respectively. Therefore, the reversible capacity of graphite was designed to be approximately 13% larger than that of NMC.

The AC impedance of the Nico-Ichi-type cell was measured at the end of the charge at C/8 every 50 cycles. As the reference (RE2 in VMP) was connected to the lithium pseudo-reference electrode, we could simultaneously obtain the impedance profiles of [WE-PRE] for the NMC cathode, [CE-PRE] for the graphite anode, and [WE-CE] for the full cell. Here, note that the obtained impedance profiles include the interfacial impedance at Li|SPE because we use the isometrically facing lithium metal as a reference.

2.4. SOC adjustment during cycle operations

In the lithium ion cell, the misalignment of the electrode-capacity window was reported as one of the factors that decrease the cell capacity [3,5,13–16]. The misalignment is derived from the irreversible loss of active lithium ions, such as through SEI formation and/or the preferential loss of the active material at either electrode. To determine the main factor causing the misalignment, we continuously monitored the voltage of the cathode at the end of discharge, V_{Cde}, at a fixed point and adjusted it to the initial value in each capacity measurement cycle (every 50 cycles) using the lithium PRE. In this case, because V_{Cde} increased with the number of cycles, an insufficient number of lithium ions were supplied (discharge for the cathode) from the reference electrode.

2.5. Electrode capacity measurement after cycle operations

After the cycle operations, the two lithium electrodes in the Nico-Ichi-type cell were disconnected at the end of discharge (2.5 V for the full cell) at the rate of C/8 with 4 h constant-voltage holding, and the capacity of each electrode was determined using the lithium counter electrode. The [Li|SPE|NMC] cell was operated starting from discharge to 2.7 V to determine the remaining capacity of the cathode, and its reversible capacity was determined at voltages between 2.7 and 4.2 V at C/8. In the same manner, the [Li|SPE|Gr] cell was operated starting from deintercalation to 2.5 V, and its reversible capacity was determined at voltages between 0 and 2.5 V at C/8.

3. Results and discussion

3.1. Initial performance of lithium ion cells with pseudo-reference electrode

As mentioned above, we can monitor the cathode and anode voltage profiles separately by introducing a pseudo-reference electrode (PRE). Fig. 3 shows the lithium ion full cell voltage and the cathode and anode individual voltage profiles of the Nico-Ichi-type [Gr|SPE|Li]–[Li|SPE|NMC] cell at C/8. The bottom axis is described on the basis of cathode capacity. We can determine the end of the charge and discharge voltages of each electrode, as shown in Fig. 3. The charge capacity is limited by the increase in cathode voltage, whereas the discharge capacity is limited by the increase in anode voltage.

Fig. 4 shows the impedance profiles of the full lithium ion cell and the cathode and anode in the Nico-Ichi-type cell at the end of charge. From the comparison between the profiles of the full cell and each electrode, we could assign the large semicircle in the low-frequency region (R_2: 12 Hz) in Fig. 4(a) to the interfacial impedance at SPE|NMC and the small semicircle in the high-frequency region (R_1: 1.3 kHz) to the interfacial impedance at Gr|SPE. The Warburg impedance observed in the full cell can be assigned to the cathode on the basis of the length of the diffusion part. Here, note that Li|SPE interfacial impedance is included in Fig. 4. For example, the semicircle in the high-frequency region in [Li|SPE|NMC] (Fig. 4(b)) overlaps with the Li|SPE interfacial impedance, and another semicircle in the high-frequency region is also derived from NMC|SPE. The corresponding small semicircle was discussed in a previous report and assigned to the SEI component [17]. To distinguish between these semicircles, we prepared a symmetrical [NMC|SPE|NMC] cell by disassembling two half cells using a lithium counter electrode in the charged state and reassembling two charged NMCs. The obtained results will be discussed in detail elsewhere.

3.2. SOC adjustment using lithium pseudo-reference electrode

We have reported the improvement in cathode reversibility with the SPE [7,18,19]. However, the lithium ion full cell (using a graphite anode) cycle performance has been found to be inferior to that using the lithium counter electrode [9]. To clarify the reason for the capacity decrease, we compared the capacity retention process under the following two conditions. We prepared two cells with the pseudo-reference electrode. In one cell, the cathode SOC was adjusted every 50 cycles. Fig. 5(a) shows the change in the voltage at the end of cathode discharge (V_{Cde}) of the cell with PRE. V_{Cde} increased from 3.54 V (1st) to 3.63 V (50th) after 50 cycles. After that, the counter electrode was connected to the lithium PRE, and the cathode was discharged (to supply lithium ions to the cathode) in the initial state (3.54 V). After the SOC adjustment, the

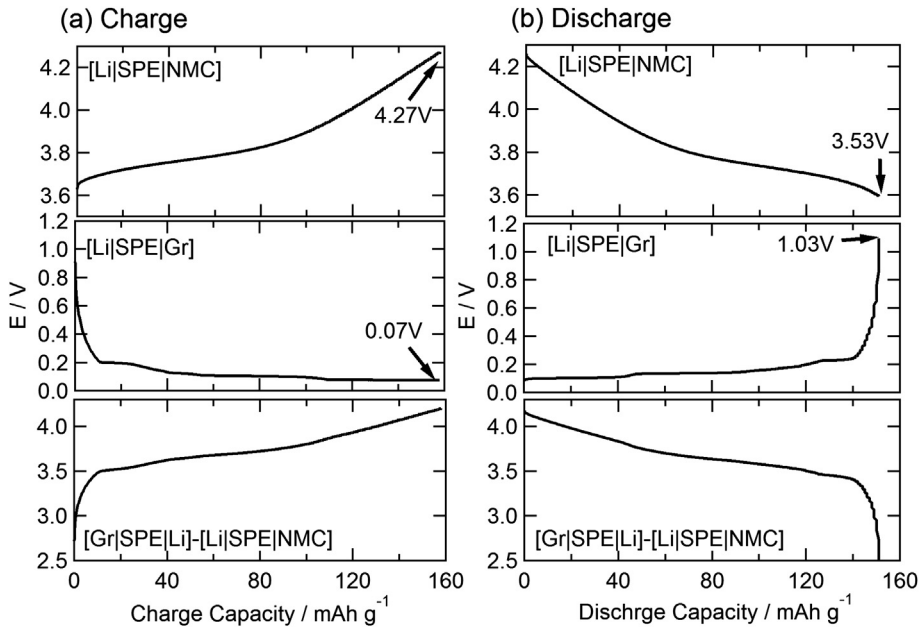

Fig. 3. Cell and individual voltage variations of Nico-Ichi-type cell. [Gr|SPE|Li][Li|SPE|NMC] at 333 K, C/8.

experiment was restarted from the 51st cycle with $V_{Cde} = 3.53$ V. The comparison of the capacity retention process of the cells with or without the SOC adjustment is shown in Fig. 5(b). The recovery of the capacity was observed in the cell with the SOC adjustment, whereas a monotonic capacity decrease was observed in the cell without the SOC adjustment. The recovery of the capacity by the SOC adjustment strongly indicates that the irreversible loss of active lithium ions rather than the loss of the active cathode material is the dominant factor causing the capacity decrease during cycle operations. In other words, an irreversible loss of lithium due to

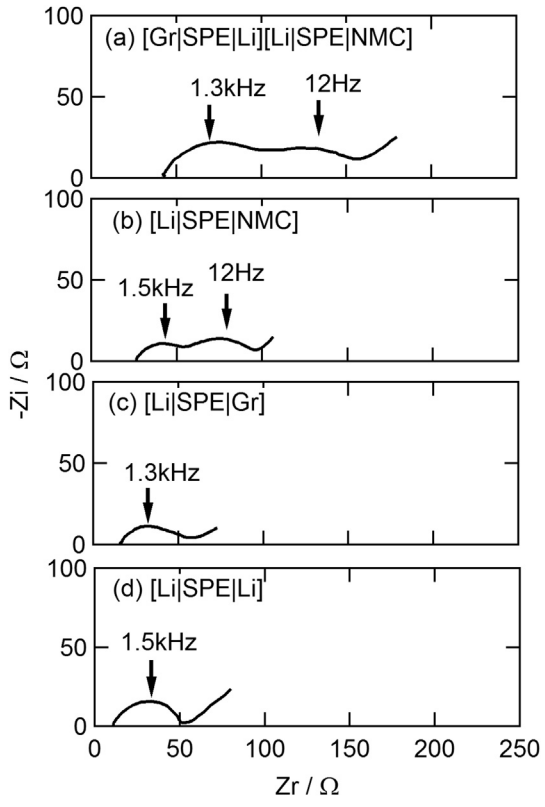

Fig. 4. AC impedance profiles of full cell (Nico-Ichi-type), and each electrode interfacial impedance at the end of charge. (a): [Gr|SPE|Li][Li|SPE|NMC], (b): [Li|SPE|NMC], (c): [Li|SPE|Gr], and (d): [Li|SPE|Li].

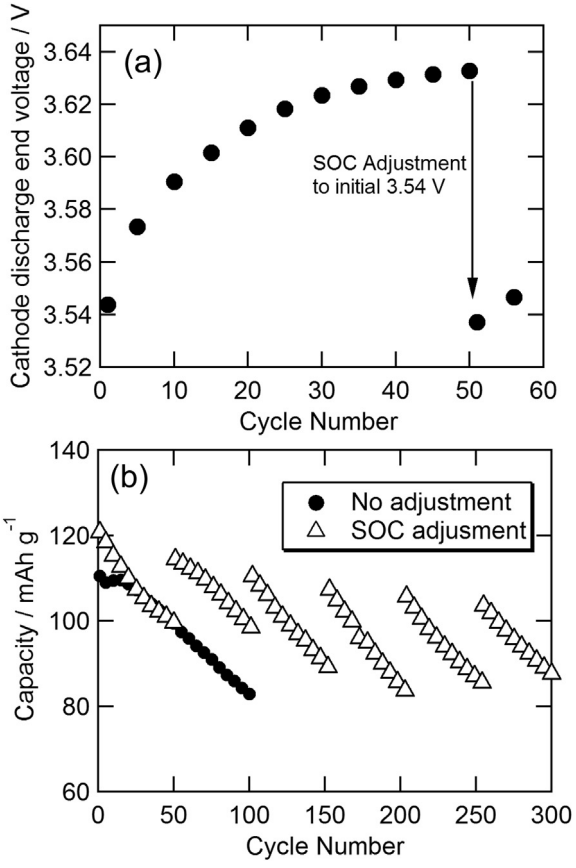

Fig. 5. (a) Variation of the voltage of cathode of the cell at the end of discharge and (b) capacity retention of full cells with and without SOC adjustment.

continuous SEI formation occurs at the graphite anode. Similar phenomena have been reported in a liquid electrolyte system with $LiNi_{0.8}Co_{0.1}Al_{0.1}O_2$ [5], $LiNi_{1/3}Mn_{1/3}Co_{1/3}O_2$ [13], $LiFePO_4$ [14,15] or $LiMn_2O_4$ [16] with graphite. We have also reported a shift to a higher SOC in a mixture cathode ($LiMn_2O_4$/$LiNi_{0.8}Co_{0.15}Al_{0.05}O_2$) with a graphite system [20]. In general, a stable SEI is formed at the anode by the reduction of liquid electrolyte components such as EC or additives such as vinylene carbonate (VC). However, we used the SPE instead of a liquid electrolyte in our system; thus, the formed SEI might not have been very stable because there was no carbonate ester such as EC or VC to form a stable SEI in the SPE structure.

3.3. Long cycle operation with pseudo-reference electrode

As mentioned above, we observed the individual voltage profiles and impedances of the cathode and anode, and followed the shift in SOC by monitoring the voltage of the cathode at the end of discharge. Then, we attempted to observe the long cycle performance of the capacity decrease with an optimized cell preparation process using the Nico-Ichi-type cell. Fig. 6(a) shows the capacity retention of a 1200-cycle operation with and without the pseudo-reference electrode (PRE). Although a slightly higher capacity was observed in the normal cell owing to its lower internal impedance, there was no significant difference in cycle performance between the normal and Nico-Ichi-type cells. This indicates that the introduction of lithium metal between the cathode and anode has little effect on cycle life. However, a shift to a high SOC in the cathode is still observed in Fig. 6(b).

Another important factor causing the degradation of cell performance is the increase in internal impedance. To determine the degradation element in the cell, we monitored the change in impedance with the number of cycles using the Nico-Ichi-type cell, as shown in Fig. 7. The equivalent circuits used for the fitting of the results are also shown in Fig. 7(d). The change in the impedance components with the number of cycles is shown in Fig. 8. R_2 components, which could be attributed to the NMC|SPE interface, clearly increase with the number of cycles. This indicates that the increase in cell impedance with the number of cycles is due to the NMC|SPE interface, probably as a result of the partial oxidation of the SPE. The decrease in R_s in [Li|SPE|NMC] can be explained by the decrease in the molecular weight of the SPE film due to the oxidation at the NMC|SPE interface, because R_s in [Li|SPE|NMC] decreased with the number of cycles and that in [Li|SPE|Gr] hardly changed. Details of the change in the molecular weight of the SPE during the cycle operation will be discussed elsewhere [11]. R_1 in [Li|SPE|NMC] increased with the number of cycles. R_1 consisted of the high-frequency semicircle of NMC [17] and the interfacial impedance at the Li|SPE interface. Therefore, we cannot yet determine the reasons for the increase in R_1 in [Li|SPE|NMC] at present.

On the other hand, the interfacial impedance in [Li|SPE|Gr] did not change significantly within 1200 cycles. The reported charge transfer impedance between the second and first stages, which corresponded to our measurement region, also did not significantly change [21]. However, continuous SEI formation occurred at the interface, which led to the increase in interfacial impedance, as mentioned above. We measured the AC impedance between 200 kHz and 50 mHz. However, we need to obtain a much lower frequency for observing the change in diffusion impedance in detail.

3.4. Determination of degradation factor

After the 100-cycle and 1500-cycle operations of the Nico-Ichi-type cells, we compared the capacity of each electrode and the misalignment of the electrode-capacity window between the cathode and anode, as shown in Fig. 9. The full scale of the *x*-axis (0–

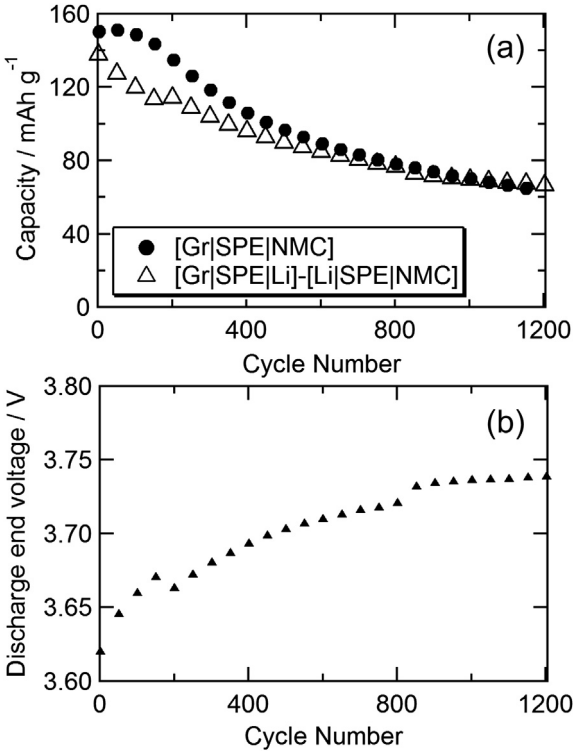

Fig. 6. (a) Cycle performance of full cells with and without PRE, and (b) voltage of cathode of cell at the end of discharge with PRE.

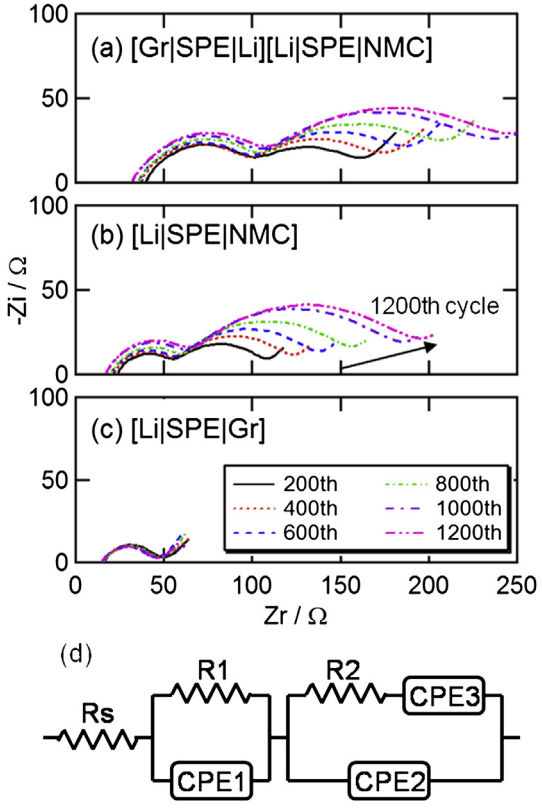

Fig. 7. Variations in AC impedance with number of cycles at the end of charge in (a) [Gr|SPE|Li]–[Li|SPE|NMC], (b) [Li|SPE|MMC], (c) [Li|SPE|Gr], and (d) equivalent circuits used for the fitting.

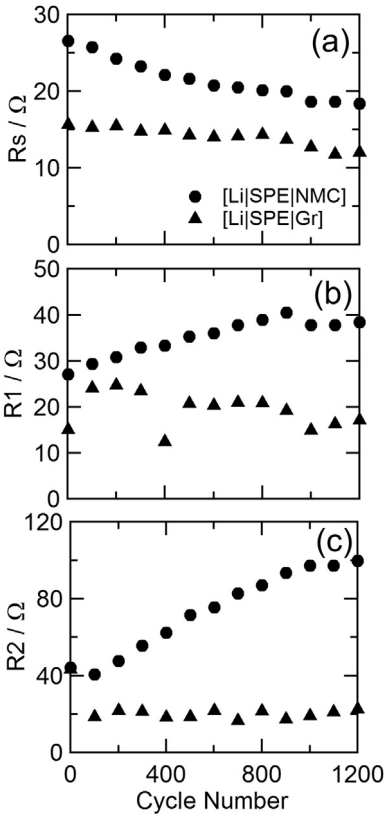

Fig. 8. Impedance variation of each component.

200 mAh g^{-1} for the cathode, and 0–400 mAh g^{-1} for the anode) is plotted by considering the loaded cathode/anode weight ratio (2/1) and each reversible capacity. The misalignment of the cathode- and anode-capacity windows is quantitatively reflected in the experimental results below. The reversible capacities of the cathode and anode are an indicator of the compatibility of the cathode and anode with the SPE. On the other hand, the misalignment of the electrode-capacity window, which is specifically the decrease in usable capacity due to the shift in the operated SOC, is an indicator of the irreversible loss of active lithium ions in operation, as mentioned above [3,5,13–17]. Table 1 and Fig. 9 show a summary of the cathode reversible capacity (C_{rev}), the shifted capacity from the 2.5 V full cell disassembly (C_{shift} denoted by ▲), the anode reversible capacity (A_{rev}), the shifted capacity of the anode (A_{shift}), and the full-cell reversible capacity (T_{rev}) after formation, 100 cycles, and 1500 cycles. Here, the cathode reversible capacity (C_{rev}) was estimated in the voltage range between 3.0 and 4.2 V. On the other hand, the full cell was operated between 2.5 and 4.2 V; thus, the actual operated cathode capacity was slightly larger than C_{rev}, because the cathode in the full cell was charged over 4.2 V. Then, we defined the additional cathode capacity ($C_{>4.2\ V}$ denoted by ▽). The observed voltage of the cathode at the end of charging in the full cell was 4.25 V (▽ = 5 mAh g^{-1}) at the formation and after 100 cycles, and 4.30 V (▽ = 10 mAh g^{-1}) after 1500 cycles.

The reversible capacity of the cell (T_{rev}) decreased from 137 mAh g^{-1} (formation) to 121 mAh g^{-1} (100 cycles) as calculated from the cathode weight. However, the reversible capacity of the cathode (C_{rev}) exhibited no significant change (decreased capacity, C_{deg} denoted by ▼ = 2 mAh g^{-1}). Although the anode capacity decreased by 5 mAh g^{-1} after 100 cycles, the decrease corresponds to only 2.5 mAh g^{-1} for the full cell, because the active material weight ratio of graphite to NMC is approximately 1:2. This indicates that the capacity decrease of the cell could not be explained by only the capacity decrease of the electrodes. Here, the open circuit potential (OCP) of the cathode after disconnecting the full cell at 2.5 V increased from 3.67 to 3.70 V owing to the irreversible loss of lithium at the graphite anode. The loss of active lithium ions is reflected in the shifted capacity of the cathode (C_{shift} denoted by ▲), as mentioned previously. Note that the calculated cathode operated capacity, $C_{rev} - C_{shift} + C_{>4.2\ V}$ (△+▽ = 120 mAh g^{-1}), could almost explain the reversible capacity (T_{rev} = 121 mAh g^{-1}) of the full cell. Therefore, the shift of the cathode due to the irreversible loss of lithium at the anode is a dominant factor causing the capacity decrease of the full cell after 100 cycles. Similarly, the reversible capacity of the full cell after 1500 cycles (T_{rev} = 62 mAh g^{-1}) could almost be explained by $C_{rev} - C_{shift} + C_{>4.2\ V}$ (△+▽ = 62 mAh g^{-1}). Here, the dominant degradation factor is still the shift of the cathode (▲ = 69 mAh g^{-1}). However, the capacity decrease of the cathode (▼ = 30 mAh g^{-1}) also contributes to that of the cell. The increase in the voltage of the cathode at the end of charging in the full cell may induce the decrease in cathode reversible capacity. The capacity decrease of the cathode after 1500 cycles may be explained by the increase in the operation voltage range of the cathode.

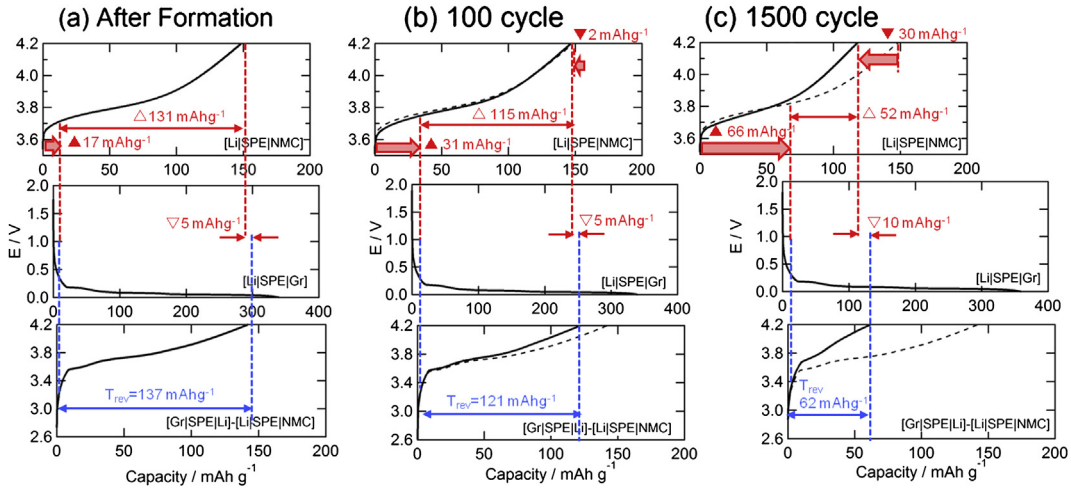

Fig. 9. Electrode capacity and misalignment of electrode-capacity window before and after cycle operation.

Table 1
Capacity retentions of the cathode, anode, and lithium-ion full cell configuration in [Gr|SPE|Li]–[Li|SPE|NMC] "Nico-Ichi" type cell at formation cycle, after 100 cycles and after 1500 cycles.

Capacity	Cathode/mAhg^{-1}				Anode/mAhg^{-1}			Full cell/mAhg^{-1}		
Components	C_{rev} (C_{deg} ▼)	C_{shift} ▲	$C_{>4.2\ V}$ ▽	OCP/V	A_{rev}	A_{shift}	OCP/V	Calc. △ + ▽	Exp. T_{rev}	OCV/V
Formation Cycles	148	17	5	3.67	345	5	1.14	136	137	2.53
100 cycles	146 (2)	31	5	3.70	340	8	1.18	120	121	2.52
1500 cycles	118 (30)	66	10	3.78	350	13	1.22	62	62	2.56

▼: Decrease of cathode reversible capacity (C_{deg}), ▲: Shifted capacity (C_{shift}), ▽: Cathode capacity over 4.2 V ($C_{>4.2\ V}$), △: $C_{rev} - C_{shift}$.

As mentioned above, the most dominant factor causing the capacity decrease in the full cell is the shift of the cathode operation range due to the irreversible loss of lithium at the graphite anode. The decrease in cathode reversible capacity is a secondary factor causing the cell capacity decrease, and it was accelerated by the increase in the operation range after a long cycle operation. On the other hand, the reversible capacity of the anode showed no significant change after a 1500-cycle operation. However, the irreversible capacity loss at the 1500th cycle (66 mAh g^{-1}) was larger than the difference between the theoretical capacity and observed reversible capacity of the graphite anode at the 1500th cycle (372–350 = 22 mAh g^{-1}). This indicates that irreversible lithium compounds in graphite did not occupy the active sites inside the graphite layer but accumulated at the graphite surface similarly to SEI.

4. Conclusion

We proposed a simple and novel procedure for introducing a pseudo-reference electrode (PRE) into the cathode and anode by externally connecting an array of pair-type cells, i.e., [Gr|SPE|Li]–[Li|SPE|NMC] (named the Nico-Ichi-type cell), and we determined the capacity decrease of a solvent-free lithium ion polymer battery. The proposed lithium ion full cell with the PRE exhibited stable performance similar to that of a conventional lithium ion full cell without the PRE. We obtained the following results concerning the capacity decrease of the full cell.

1. The most dominant factor causing the capacity decrease during cycle operation was the continuous irreversible loss of lithium at the graphite anode in our system.
2. The decrease in NMC cathode reversible capacity was the secondary factor causing the capacity decrease of the cell; it was accelerated by an increase in the operation range after a long-cycle operation.
3. The graphite anode exhibited a stable reversible capacity during continuous SEI formation.
4. Although the oxidation of the SPE was observed from the increase in interfacial impedance at the SPE|NMC interface by AC impedance analysis, the oxidation of the SPE was not the dominant factor causing the capacity decrease.

The reversibility over 1000 cycles obtained using the 4 V class NMC, polyether-based dry SPE, and graphite is the best performance for a long cycle operation to the best of our knowledge. The formation of a stable protection layer that minimizes the loss of lithium at the graphite anode is the route that should be given the highest priority to obtain long-life lithium ion cells with the SPE. We consider that the proposed system is the best method of realizing "safe" all-solid-state batteries in the near future.

References

[1] K. Amine, C.H. Chen, J. Liu, M. Hammond, A. Jansen, D. Dees, I. Bloom, D.G. Henriksen, J. Power Sources 97–98 (2001) 684–687.
[2] Y. Kobayashi, H. Miyashiro, K. Kumai, K. Takei, T. Iwahori, I. Uchida, J. Electrochem. Soc. 149 (2002) A978–A982.
[3] D.P. Abraham, S.D. Poppen, A.N. Jansen, J. Liu, D.W. Dees, Electrochim. Acta 49 (2004) 4763–4775.
[4] A.K. Kercher, J.O. Kiggans, N.D. Dudney, J. Electrochem. Soc. 157 (2010) A1323–A1327.
[5] I. Bloom, A.N. Jansen, D.P. Abraham, J. Knuth, S.A. Jones, V.S. Battaglia, G.L. Henriksen, J. Power Sources 139 (2005) 295–303.
[6] J.-M. Tarascon, M. Armand, Nature 414 (2001) 359–367.
[7] H. Miyashiro, Y. Kobayashi, S. Seki, Y. Mita, A. Usami, M. Nakayama, M. Wakihara, Chem. Mater. 17 (2005) 5603–5605.
[8] S. Matsui, T. Muranaga, H. Higobashi, S. Inoue, T. Sakai, J. Power Sources 97–98 (2001) 772–774.
[9] Y. Kobayashi, S. Seki, Y. Mita, Y. Ohno, H. Miyashiro, P. Charest, A. Guerfi, K. Zaghib, J. Power Sources 185 (2008) 542–548.
[10] Y. Kobayashi, Y. Mita, S. Seki, Y. Ohno, H. Miyashiro, N. Terada, J. Electrochem. Soc. 154 (2007) A677–A681.
[11] T. Kobayashi et al., in preparation.
[12] J. Xu, S.-L. Chou, Q.-F. Gu, H.-K. Liu, S.-X. Dou, J. Power Sources 225 (2013) 172–178.
[13] I. Bloom, L.K. Walker, J.K. Basco, D.P. Abraham, J.P. Christophersen, C.-D. Ho, J. Power Sources 195 (2010) 877–882.
[14] M. Safari, C. Delacourt, J. Electrochem. Soc. 11, 158 A1436–A1447.
[15] M. Kassem, J. Bernard, R. Revel, S. Pelissier, F. Duclaud, C. Delacourt, J. Power Sources 208 (2012) 296–305.
[16] T. Tsujikawa, K. Yabuta, T. Matsushita, M. Arakawa, K. Hayashi, J. Electrochem. Soc. 158 (2011) A322–A325.
[17] P. Reale, D. Privitera, S. Panero, B. Scrosati, Solid State Ionics 178 (2007) 1390–1397.
[18] Y. Kobayashi, S. Seki, A. Yamanaka, H. Miyashiro, Y. Mita, T. Iwahori, J. Power Sources 146 (2005) 719–722.
[19] Y. Kobayashi, S. Seki, M. Tabuchi, H. Miyashiro, Y. Mita, T. Iwahori, J. Electrochem. Soc. 152 (2005) A1985–A1988.
[20] Y. Kobayashi, T. Kobayashi, K. Shono, Y. Ohno, Y. Mita, H. Miyashiro, J. Electrochem. Soc. 160 (2013) A1181–A1186.
[21] M. Itagaki, S. Yotsuda, N. Kobari, K. Watanabe, S. Kinoshita, M. Ue, Electrochim. Acta 51 (2006) 1629–1635.